Cabbel.doc
04/27/99 8:44 AM

CABBELING CATASTROPHES

Laurie Padman & Robin Muench

Earth & Space Research

1910 Fairview E., Suite 102

Seattle, WA 98102-3620, USA

Eberhard Fahrbach

Alfred-Wegener-Institut für Polar und Meeresforschung

D-2850 Bremerhaven, Germany

January 1998 Draft

for submission to

Journal of Geophysical Research - Oceans

ABSTRACT

The structure and dynamics of an active diapycnal cabbeling instability in the Weddell Sea are described. The estimated rate of heat transfer from the relatively warm pycnocline to the near-freezing surface mixed layer during the event was about 300 W m^{-2}. The observed event was initiated by differential advection of a relatively saline and dense mixed layer over a filament of anomalously warm Weddell Deep Water. Other frontal regions such as near the shelf/slope front may also provide the necessary conditions for advectively-initiated diapycnal cabbeling, as well as isopycnal cabbeling. We hypothesize that diapycnal cabbeling can also occur during periods of rapid ice growth in the central Weddell Gyre, specifically under conditions of large ice divergence. Variability in step properties in the central Gyre may also be correlated with interannual variations in seasonal ice extent.

Diapycnal cabbeling can be treated as a limiting case of diffusive convection in which external forcing, such as ice formation or differential advection, initiates the instability. After the density contrast between the surface and subsurface layers is increased, either by the process itself or by summer restratification, the layers can be maintained in a less active state by diffusive convection. During this phase, the features can be redistributed over broad areas by advection within the mean regional currents.

1. INTRODUCTION

When two water parcels with differing temperature (T) and salinity (S) mix, the mixing product is denser than the mean density of the unmixed components. This process is known as “cabbeling” (see *Foster* [1972] for a discussion and etymology), or more descriptively as “densification during mixing” [*Kil’matov and Kuz’min*, 1991]. When the initial water parcels have the same density, i.e., mixing occurs along an isopycnal, formation of a denser parcel then drives convective mixing across isopycnals. We shall refer to this process as “isopycnal cabbeling”. Various authors [e.g., *Bowman and Akubo*, 1978; *Garrett and Horne*, 1978; *Fedorov*, 1981; *Kil’matov and Kuz’min*, 1991] have studied the possible role of isopycnal cabbeling in frontal zone mixing, where the cross-frontal isopycnal gradients of θ and S, and thus the possible density changes when parcels are mixed, are large.

Even when two fluid parcels having slightly different density are mixed, under appropriate conditions (discussed below) the mixing product can be denser than either initial parcel. This gives rise to the possibility that mixing across isopycnals in a weakly stratified fluid can cause a cabbeling instability. We shall refer to this process as “diapycnal cabbeling”. Consider a two-layer ocean, where the upper and lower layer properties are denoted by (S_1, T_1, σ_1) and (S_2, T_2, σ_2), respectively, and σ_i is the potential density of layer ‘*i*’. Since the oceanic application with which we will be most concerned is the system’s sensitivity to changing surface layer salinity, we discuss our model in terms of constant T_1, T_2, and S_2. Furthermore, we also consider only the case of $S_2>S_1$ and $T_2>T_1$. This system is illustrated in T-S space in **Figure 1**, for the specific case of the Weddell Sea that was discussed by *Fofonoff* [1956] and *Foster* [1972]. The lower layer is represented by the temperature and salinity of the Warm Deep Water (WDW) at the temperature maximum: while this value actually varies both spatially and in time, we take characteristic values of (S_2, T_2)=(34.68, 0.6^{o}C). The possible upper layer properties (S_1, T_1) are assumed to lie along the freezing point temperature at the surface, T_1=T_f(S_1, P=0).

The isopycnals that are shown in **Figure 1** are taken relative to 120 m, the mean depth of the interface in the example to be discussed later. With the small vertical density differences that occur in cabbeling-favorable regions, the pressure dependence of the thermal expansion coefficient in the equation of state can play an important role in the interpretation of the water column's true stability to cabbeling [*Foster*, 1994].

In order to maintain static stability, i.e., $\sigma_1<\sigma_2$, the surface layer salinity, S_1, must lie to the left of the isopycnal (σ_2). As *Fofonoff* [1956] noted, the critical condition for cabbeling is that some mixing ratio between the two layers can lead to production of water that is denser than σ_2. This condition requires that the mixing line between the two layers is steeper than the tangent to isopycnal σ_2 at (S_2, T_2). Following *Walin* [1993], we denote the two critical salinities as S_0 and S_*, where

$$\rho(S_0, T_1)=\rho(S_2, T_2), \tag{1}$$

and

$$(T_2-T_1)=(S_2-S_*)/(\mathrm{d}T/\mathrm{d}S)_2\ . \tag{2}$$

In (2), $(\mathrm{d}T/\mathrm{d}S)_2$ is the slope of the tangent to the isopycnal, σ_2, at the point (S_2, T_2). Hence, S_* represents the lowest surface layer salinity that allows the density of some mixing product to exceed σ_2, while S_0 is the highest surface layer salinity that maintains the static stability of the two-layer system.

The system that has been defined is consistent with, but more restrictive than, the necessary conditions for diffusive convection [*Turner*, 1973; *Schmitt*, 1994]. The efficiency of diffusive convection is a function of the density ratio, R_ρ, given by

$$R_\rho = \frac{\beta \partial S / \partial z}{\alpha \partial T / \partial z}, \tag{3}$$

where β and α are the saline contraction and thermal expansion coefficients, respectively. Diffusive convection is most energetic when $R_\rho \approx 1$, i.e., where the intrinsically-unstable thermal stratification almost cancels the intrinsically-stable salinity stratification in the equation of state. The slope of the tangent to σ_2 at (S_2, T_2) is equal to $\alpha(S_2, T_2)/\beta(S_2, T_2)$, and thus $R_\rho(S_2, T_2)\leq 1$ for $S_1 \geq S_*$.

Isopycnal curvature is primarily due to the change in α as a function of T, and the existence of a finite range of cabbeling-favorable surface layer salinities, $S_* < S_1 < S_0$, requires that $\alpha(T_1) < \alpha(T_2)$. For diapycnal cabbeling to be initiated, it is also necessary that the interface separating the two layers be sufficiently thin that mixing can occur between the two layers. These conditions are most easily met in the cold, weakly stratified, high-latitude oceans, in regions that might therefore also be sensitive to deep convection driven by surface cooling and brine rejection during ice formation. In these regions, such as the central Greenland Sea and the Weddell Gyre, the stratification consists of a fresh, near-freezing surface layer overlying a weakly stratified, but warmer and more saline, deep layer. This is the context in which *Walin* [1993] investigated sea ice development over deep, weakly stratified water, and is the type of stratification to be studied in the present paper.

Walin [1993] tentatively concluded that cabbeling, as a mechanism for creating vertical mixing, was not likely to significantly influence the ice growth, which he treated as essentially a thermodynamic balance between entrainment of the Warm Deep Water (WDW) by surface stress and brine rejection, and heat flux through the ice to the atmosphere. His conclusion was based, in part, on the lack of observational evidence for the existence of the cabbeling instability as a process that is distinct from diffusive convection. Laboratory and theoretical work by *McDougall* [1981a,b] supported the view that, when stratification is cabbeling-favorable, double-diffusion is actually the dominant heat and salt transport process. *Rudels* [1991] reached a similar conclusion. Nevertheless, T-S structure in the Weddell Gyre is frequently consistent with marginally cabbeling-favorable conditions, $S_{SML} \approx S_*$ [*Fofonoff*, 1956; *Foster*, 1972; *Foster and Carmack*, 1976].

What has been missing so far is observational evidence that diapycnal cabbeling really does occur in the ocean as a process that is distinct from diffusive convection. In cabbeling, formation of dense water that drives lower-layer convection can occur with constant diffusivities for T and S. In the classical view of double-diffusion (see, e.g., *Linden and Shirtcliffe* [1978] and *Padman and Dillon* [1989]), convection is driven by the formation of dense boundary layers at the interface, resulting from the different diffusivities of T and S, denoted K_T and K_S respectively. As *Walin* [1993] noted, *McDougall* [1981a,b] only considered the situation where the heat and salt fluxes through the interface were determined solely by the stratification and the double-diffusive (i.e., $K_T \neq K_S$) instability. In these studies, since double-diffusion was the primary source of the interface fluxes, it is not surprising that the system evolved in a manner consistent with double-diffusion. In the ocean, however, mixing within the interface may also be due to shear instabilities, or a response to turbulence within the surface layer that is due to stress and buoyancy forcing at the ocean surface rather than diffusive convection. These latter processes are expected to have similar diffusivities for T and S, and thus the applicability of *McDougall's* work to the ocean context is not yet determined.

Diffusive convection is, certainly, an active process in the Weddell Gyre [*Foster*, 1972; *Foster and Carmack*, 1976; *Muench et al.*, 1990; *Rudels*, 1991; *Robertson et al.*, 1995], and it is not easy from typical CTD observations to distinguish between profiles that would indicate "normal" diffusive convection from those that suggest active cabbeling. Part of the difficulty arises from a poor theoretical understanding of the likely structure of the cabbeling instability, although *Foster* [1972] provided some guidance through a two-dimensional linear instability analysis. In this paper we present recent evidence that the diapycnal cabbeling instability does occur in the Weddell Sea, and discuss the oceanic conditions that are necessary for cabbeling (section 2). We then briefly discuss the basin-scale implications for this process (section 3), and summarize our findings in section 4.

2: A CABBELING EVENT IN THE EASTERN WEDDELL SEA

2.1. Oceanographic and Experimental Setting

An intensive small-scale physical measurement program ("**ANZFLUX"**: the Antarctic Zone Flux Experiment) was carried out from the U.S. icebreaker *N.B. Palmer* in the austral winter (July/August) of 1994, in the eastern Weddell Sea [*McPhee et al.*, 1996; *Flanagan and Yulsman*, 1996]. The program's primary goal was to measure the upward flux of oceanic heat and its interaction with the sea ice and atmosphere in winter, in a region that is believed to be very sensitive to climate variability. Two camps were established on the mobile pack ice. The second camp, which is the focus of this paper, drifted over the eastern flank of Maud Rise, a submarine plateau centered near 65°S, 3°E (**Figure 2a)**. The hydrographic conditions in this region are extremely complex [*Bersch et al*., 1992; *Fahrbach et al.*, 1998; *Muench et al.*, 1998], but the dominant feature is a Taylor column over the Rise [*Ou*, 1991]. The water within the column is strongly upwelled, with up to 400 m elevation of deep isopycnals [*Bersch et al*., 1992]. The relative isolation of the fluid within the column creates anomalous hydrographic conditions: the winter mixed layer is salty and therefore dense compared to the surrounding ocean, and the overall static stability is much lower than outside the column [*Gordon and Huber,* 1990]. The large-scale mean flow of WDW near the Rise, based on tracing core layer properties, is towards the southwest, i.e., it is part of the southern limb of the clockwise-flowing Weddell Gyre [*Orsi et al.*, 1993]. Mean currents from moorings [*Bersch et al.,* 1992] confirm this circulation pattern. *Fahrbach et al*. [1998] suggested that a total volume transport of about 18 Sv (where 1 Sv=10^6 m^3s^{-1}) flows generally westward in the vicinity of Maud Rise. Of this total, about 14 Sv circulates around the northern slope, and about 4 Sv around the southern slope. This flow regime creates a "halo" of warm WDW (T_{max}>1°C) surrounding the cold (T_{max}<0.6°C) Taylor column over the center of the Rise [*Bagriantsev et al*., 1989]. Several programs, including **ANZFLUX,** have found that the hydrographic conditions west ("downstream") of Maud Rise are extremely variable in both time and space, suggestive of a wake associated with mesoscale instabilities of the complex Maud Rise current system. It is also possible that some of the variability arises from the intermittent separation of the Taylor column itself, possibly during periods of stronger mean flow [*Ou*, 1991]. The anomalous fluid may then be advected westward by the mean Gyre circulation.

The drift track of the **ANZFLUX** Maud Rise ice camp (**Figure 2b**) shows significant variations in both speed and direction; this ice drift is highly correlated with wind velocity [*McPhee et al*., 1996]. The mean ice drift was eastward, away from Maud Rise, and thus the wind-forced camp motion allowed us to obtain data over the transition region east of the Taylor column. Three sample profiles of T, S, and σ_0 illustrate some of this variability (**Figure 3**). Many hydrographic profiles during the **ANZFLUX** Maud Rise drift included one or more thick, subsurface, quasi-homogeneous layers, e.g., CTD-108. The locations of thick layers below the surface layer for the entire Maud Rise drift in **ANZFLUX** are shown in **Figure 4**, using the vertical temperature gradient, $T_z(t,z)$, based on data from a rapidly-sampled microstructure profiler (see section 2.2, below), as an indicator of step location. Layers correspond to regions of $T_z \approx 0$ within the pycnocline. In space (**Figure 5**), these layers are found where the WDW has a relatively high T_{max}, and the surface layer salinity, S_{SML}, is relatively high. The pycnocline within this region is typically about 50 m shallower than on either side (**Figure 4**). We do not know, however, whether the processes that are responsible for the subsurface layers are also directly involved in raising the pycnocline, or if these two processes are simply coincident in this region. A raised pycnocline is typical of the extensive "warm pool" found on the northwestern edge of Maud Rise during the **ANZFLUX** mesoscale survey [*Muench et al*., 1998], and this is believed to be a direct response to the Taylor column circulation [*Ou*, 1991].

2.2. Observations of a Cabbeling Event

The instrumentation systems that we will use to describe the cabbeling event are summarized by *McPhee et al*. [1996], *Stanton et al.* [1998], and a series of articles in the 1995 review edition of the *Antarctic Journal of the U.S.*, and will therefore be only very briefly described here. An ice-mounted mooring line supported an array of 23 temperature sensors, five conductivity/temperature sensors, and four pressure sensors [*Padman et al*., 1995]. Sensors spanned an approximate depth range of 1 to 300 m below the ice base, and sampled every minute. Actual sensor depths, which varied with the ocean-relative ice speed due to drag on the sensors and mooring line, were determined by fitting of a simple mooring model calibrated with the four pressure sensors. Microstructure profiles were obtained with the OSU Rapid-Sampling Vertical Profiler ("RSVP") [*Padman et al*., 1995; *Robertson et al*., 1995]), about every 15-20 minutes and covering the depth range from the surface to about 350 m. The RSVP provides temperature and velocity shears ($\partial u/\partial z$ and $\partial v/\partial z$) with depth resolution of 3-5 cm, plus conductivity (and thus also salinity and density) on coarser vertical scales of about 20 cm. The velocity shears can be used to generate estimates of the dissipation rate of turbulent kinetic energy, ε (see *Gregg* [1987] for a review of this procedure), while the thermal microstructure gives a clear view of the structure of convective or otherwise turbulent events. Finally, the ship-mounted 150 kHz narrow-band acoustic Doppler current profiler (ADCP) provides currents every 8 m from about 28 m to near 300 m depth. The effective time resolution on the ADCP during **ANZFLUX** was about one hour: higher-frequency signals were rarely sufficiently energetic to be seen above the ADCP's noise floor.

The thickest steps are found near t=216.9 and t=218.5 (see **Figure 4**). The former period is dominated by an intense baroclinic feature, which was clearly seen in velocity profiles from the ADCP. The latter "event" has no visible signature in the ADCP record, and might therefore represent a more typical event within the Weddell Gyre, which is largely barotropic [*Orsi et al*., 1993]. During this event, the ice camp drifted roughly northwards at about 30 cm s^{-1} (see **Figure 2**). The salinity and temperature in the surface mixed layer ("SML") are shown in **Figure 6a** for the 12-h period 218.3<t<218.8. These parameters (S_{SML} and T_{SML}) were measured every minute at 1 m below the ice base with a Seacat CTD. T. Stanton of the Naval Postgraduate School kindly provided these data. **Figure 6b** shows $T(t,z)$ for this period, based on temperature sensors located at approximately 10 m depth intervals on the mooring. Temperature between 100 and 250 m depth decreases rapidly near t=218.54. Closer inspection shows considerable variability in T throughout the active mixing period following this transition. The standard deviation of T during this period (218.55<t<218.63) is about 0.03^{o}C at each of the sensors between 125 and 190 m (**Figure 6c**). There is an approximately 15-30 minute time scale to temperature variability in this depth range, which is also seen in isopycnals above and below the mixing patch.

The T-S structure for two CTD profiles taken before and during this event demonstrate the subtle, but important, changes in the SML properties that occur during this time (**Figure 7**). At t=218.33 (yo-yo-CTD 105), S_{SML} is slightly less than S_* based on the WDW properties, then rises by 0.015 psu to 34.497 psu by t=218.41 (**Figure 6a**). This value corresponds to $S_{SML}=S_*$ (**Figure 7**). The observed subsurface layer thickness then increases rapidly (**Figure 6b**), however S_{SML} remains approximately constant. The T-S structure at t=218.58 (yo-yo-CTD 108), when the subsurface layer is thickest, shows that the T-S properties of the interface closely follow the tangent to the isopycnal passing through the original, thinner, subsurface layer. That is, this set of observations is consistent with a cabbeling event occurring just as the critical criterion ($S_{SML}=S_*$) is reached by the increase in S_{SML}.

During the same period, we obtained ten RSVP profiles. The velocity shear can be used to estimate ε from

$$\varepsilon = \frac{15}{2}\nu\left\langle(\partial u/\partial z)^2\right\rangle . \tag{4}$$

In (4), ν is the kinematic viscosity, and the factor 15/2 results from assuming that the turbulence is isotropic over the wave number range containing most of the velocity shear [*Gregg*, 1987]. The buoyancy flux, B_ρ, can then be estimated as

$$B_\rho=\Gamma\varepsilon , \tag{5}$$

where Γ is the "mixing efficiency". When the buoyancy flux is a consequence of shear production, Γ is frequently taken to be about 0.2, although values from 0.05 to 0.7 have been reported [*Moum*, 1996]. When the buoyancy flux is actually responsible for the turbulence, as in diffusive convection, $\Gamma \approx 1$ [*Taylor*, 1988]. Diapycnal cabbeling relies on other processes to initiate the mixing in the interface, but ultimately becomes unstable through a convective instability. Therefore, the appropriate value of Γ is expected to lie somewhere in the range $0.2<\Gamma<1$. The diapycnal eddy diffusivity (K_d) is simply the ratio of density flux to mean density gradient, therefore $K_d=\Gamma\varepsilon/\langle N^2\rangle$, where N is the buoyancy frequency.

The most energetic RSVP profile during the event at t=218.64 is shown in **Figure 8**. The first panel shows measured T at 4 cm resolution, and also the "Thorpe-reordered" profile, $T_{thorpe}(z)$. Only temperatures between -0.2°C and +0.4°C are shown, thus concentrating on the largest subsurface layer. The reordering process involves rearranging the measured discrete set of $T(z)$, $\{T_i: i=1,n\}$, such that $T_{i+1}>T_i$ for all i [*Thorpe*, 1977; *Dillon*, 1982]. One critical assumption for us is that density is a monotonic function of T, thus reordering is only performed for data above the WDW temperature maximum. The reordered profile represents the profile that would result from adiabatic settling of an observed profile containing statically-unstable regions. With these assumptions, the difference between the measured and reordered profile at a given depth represents some measure of the thermal variability due solely to turbulence, and excludes variations due to reversible processes such as internal waves. Furthermore, the vertical gradient, $\partial T_{thorpe}/\partial z$, can be used as an estimate of the "mean" background temperature gradient prior to the onset of the turbulent event.

The second panel in **Figure 8** shows S and σ_0 averaged over 1 m for the same profile. Much of the noise in these profiles results from the difficulty of accurately matching the response functions for the microscale T and C sensors in this environment. The third panel shows ε, which exceeds the noise floor of about $3\mathrm{x}10^{-9}$ m^2s^{-3} (dashed line) in the mixed layer, the pycnocline, and the upper portion of the subsurface layer. We will use the pycnocline-averaged value of ε below to estimate the heat flux through the pycnocline and into the SML.

The rapid ice drift during this period (~30 cm s^{-1}) precludes unequivocal separation of spatial structure from temporal variability. Comparisons of nearly-simultaneous profiles of T from the mooring, the OSU profiler, and the LDEO CTD demonstrate that hydrographic properties can vary significantly over the approximately 200-300 m horizontal distance separating each of these measurement sites. Thus, variability that we measure at a single location includes lateral advection of horizontal property gradients.

We summarize our observations below: the uppermost subsurface layer is denoted 'L_2'.

a) Salinity at 1 m depth increased by about 0.015 just prior to the observed thickening and cooling of L_2. Temperature at 1 m increased by about 0.03^{o}C at the end of the event (**Figure 6a**).
b) Within the event, the *T-S* profile is marginally favorable for cabbeling, i.e., $S_{SML} \geq S_*$ (**Figure 7**).
c) The mean dissipation rate across the pycnocline during this event is about 10^{-8} m^2 s^{-3}, which, for Γ=0.2 (see (5)), corresponds to a diffusivity of about 10^{-4} m^2 s^{-1} and a heat flux of 65 W m^{-2}. If $\Gamma \approx 1$, $K_d \approx 5\text{x}10^{-4}$ m^2 s^{-1}, and the heat flux through the pycnocline is about 300 W m^{-2}.
d) There is an approximately 20-minute time scale to thermal variability in L_2, which is also seen in the pycnocline displacements below the layer (**Figure 6b**).
e) The mean vertical thermal gradient within L_2 is about 0.001^{o}C m^{-1}, based on the rapidly-sampled thermistor chain. Thorpe re-ordering of the most energetic RSVP profile taken during this period (**Figure 8a**) shows a similar mean gradient.
f) The standard deviation of temperature at the sensors within L_2 is about 0.03^{o}C at each level. The standard deviation of temperature differences between the observed profile and the Thorpe-reordered profile (**Figure 8a**) within L_2 is about 0.015^{o}C.
g) The observed cooling in L_2 requires the entrainment of about 20 m of pycnocline and SML fluid.

If we interpret the rise in T_{SML} after t=218.64 as a response to the observed event, the required time-integrated heat flux from the pycnocline to the surface layer is about 8x10^6 J. The pycnocline heat flux ($F_{H,pyc}$) estimated from profiles of ε and using Γ=0.2 in (5), is 65 W m^{-2}. With this flux, it would take about 2 days to cause the observed mixed layer warming. However, if $\Gamma \approx 1$, i.e., the observed dissipation is a response to the buoyancy flux due to cabbeling, then $F_{H,pyc} \approx 300$ Wm^{-2} and the required heating takes about 6 h, which is comparable with the observed event duration. Our interpretation is obviously complicated by the possibility that horizontal advection is responsible for the presence of the warm SML near the mixing event within the pycnocline. We also note that the sampling interval for the RSVP profiles is about 15-20 minutes, which is insufficient to fully resolve the time scales within the turbulent event. It is quite possible that our profiles have missed the critical flux events that determine the average value over this feature [*Baker and Gibson*, 1987].

Estimates of the vertical heat flux within the layer itself ($F_{H,L}$) can now be made. First, assume that $F_{H,L} \approx \rho c_p \langle T'w' \rangle$, where T' and w' are turbulent temperature and vertical velocity scales. We approximate $\langle T'w' \rangle$ by $c\sigma_{T'}\sigma_{w'}$, where $\sigma_{T'}$ and $\sigma_{w'}$ are the standard deviations of T' and w' respectively, and c is the squared coherence between T' and w'. An estimate of w' can be obtained by noting that the time scale (τ) for convective eddies in the layer is approximately 20 minutes, and the length scale for a typical eddy (L_{eddy}) is about 10 m, based on visual inspection of the profiles of (T-T_{thorpe}). Then $w' \approx L_{eddy}/\tau$, which is about 1 cm s^{-1}. For c=1, we then obtain $F_{H,L} \approx 600$ W m^{-2}.

An alternative approach is to estimate the eddy diffusivity in the layer, K_L, then obtain $F_{H,L}$ from $F_{H,L} = \rho c_p K_L \langle T_z \rangle_L$, where $\langle T_z \rangle_L$ is the mean temperature gradient in the clearly turbulent core of the layer. We follow *Deardorff and Willis* [1987], writing $A_L = 0.07 w_* H_L$, where A_L is the layer eddy viscosity, and $w_* = (B_\rho H_L)^{1/3}$ (see also, *Padman* [1994]). We assume that the buoyancy flux, B_ρ, is equal to the flux through the pycnocline at the top of the layer, and furthermore that $\langle B_\rho \rangle \approx \langle \varepsilon \rangle$. With these assumptions, for $\varepsilon = 10^{-8}$ m^2 s^{-3} and H_L=80 m, we obtain $w_* \approx 1$ cm s^{-1}, and $A_L \approx 0.06$ m^2 s^{-1}. Now, *Padman* [1994] suggested, for an active diffusive-convective layer, that the Prandtl number, $Pr = A_L/K_L$, was about 3, although in high Reynolds number turbulence, we expect $Pr \approx 1$. Taking these limits, we obtain $0.02 \le K_L \le 0.06$ m^{2}s^{-1}, and the resultant heat flux when $\langle T_z \rangle_L = 0.001^\circ$C m^{-1} is $85 < F_{H,L} < 250$ W m^{-2}.

The vertical velocity scale of 1 cm s^{-1} and the apparent time scale of 20 minutes are intriguingly close to the analytical model solutions of *Foster* [1972]. These solutions were obtained from a two-dimensional stability analysis for initially neutral stability, i.e., $\sigma_1(t=0)=\sigma_2(t=0)$, with the assumption that the eddy diffusivity and viscosity in the interface are both 10^{-4} m^{2}s^{-1}. We have repeated *Foster's* stability analyses for varying S_{SML}, and find that, for only weakly cabbeling-favorable conditions (i.e., $S_{SML} \approx S_*$), the growth time scale is approximately doubled and the maximum vertical velocity is approximately halved relative to the neutral-stability case.

We now can suggest how such events occur, and how they evolve. The observed instability developed when a more saline surface layer was advected over an area of warmer, and thus slightly less dense, WDW. In *T-S* space (**Figure 7**), the Maud Rise SML with S_{SML}>34.50 is seen to be marginally cabbeling-unstable ($S_{SML}>S_*$) with respect to the filament of WDW over which it was advected. Sufficient mixing occurred between the two layers to create anomalously dense water at the bottom edge of the pycnocline. This mixing might have been due to shear-driven instabilities or energetic diffusive convection (possible since $R_\rho \approx 1$ in the lower pycnocline). At some time, the buoyancy anomaly became sufficiently large to overcome the viscous forces, and a catastrophic convective event ensued. The proposed process is directly analogous to the classic view of diffusive convection as the intermittent separation of a buoyant boundary layer when a critical boundary layer Rayleigh number is reached by diffusion [*Linden and Shirtcliffe*, 1978; *Padman and Dillon*, 1989]. In diffusive convection, however, the unstable boundary layers only develop because the effective diffusivities for heat and salt, K_T and K_S respectively, are different, which is not a necessary condition for diapycnal cabbeling. We can see that, in some ways, diapycnal cabbeling can be viewed as a limit of diffusive convection rather than as an entirely distinct process, although the imposition of a non-double-diffusive source of mixing in the interface may be critical to setting the characteristics of the developing instability.

Once the instability is initiated, active convection occurs primarily in the growing lower layer. As *McDougall* [1981a,b] proposed, diapycnal cabbeling is a form of asymmetric diffusive convection. However, our observations suggest that the cabbeling layer has entrained some of the SML and all of the pycnocline: this is required to explain the observed cooling of the layer. In the present data set, advection, mesoscale variability, and internal tides and waves prevent us from accurately assessing the heat budget for this event. Suppose, however, that the entire pycnocline (~10 m thick) and the lower 10 m of the SML, i.e., a layer of water about 20 m thick with a mean temperature of about -1.3^{o}C, is entrained into the lower convective layer, which has an initial mean temperature of about 0.4^{o}C over the 100 m thickness encompassed by the final convective event. Then the resultant final temperature will be about 0.1^{o}C. Although the observed final lower layer temperature is closer to 0^{o}C, the difference can be achieved very easily with a small adjustment to the assumed quantity of SML fluid that is entrained. The active turbulence within the pycnocline, seen in the microstructure measurements and also suggested by the above heat budget of L_2, is consistent with the process releasing sufficient heat from L_2 to provide the observed SML warming of about 0.03^{o}C. Note that cabbeling entrains upward, i.e., in the absence of competing downward entrainment, the pycnocline will become shallower. As we noted earlier, layers are found in a region where the mean pycnocline depth is about 50 m shallower than the surroundings (**Figure 4**). It is possible that upward entrainment by cabbeling is responsible for this shoaling: if so, a secondary effect of cabbeling is to raise the pycnocline closer to the surface, and thus increase the efficiency of surface stress and brine rejection in entraining WDW heat to the ice base. In this scenario, the thermodynamic balance of the ocean/ice system cannot be modeled accurately without considering the cabbeling-driven shoaling of the pycnocline, since a basic mixed layer model will deepen the pycnocline until only sporadic, energetic stress-driven events can provide additional oceanic heat flux to the ice base.

Some additional factors need to be considered when assessing the likelihood of cabbeling. First, some mechanism for preconditioning the water column to a “steppy” profile might be required, in order to provide the thin interface that then allows direct mixing of dissimilar water parcels. For thicker pycnoclines, while densification on mixing still occurs, the density of the mixing product is more likely to remain within the pycnocline. Diffusive convection is the obvious candidate to assist in creating an initial steppy structure, although energetic shear-initiated mixing can also create the finestructure that might help precondition the water column for cabbeling.

Secondly, it is possible that the time scale over which the cabbeling-favorable conditions are established at a specific location is important to the evolution of the hydrographic profile and sea ice properties. Evolution of a low-stability upper ocean when ice is present is extremely complex even where horizontal advection can be ignored

[*Martinson*, 1990; *Walin*, 1993]. Heat lost from the pycnocline is potentially available to melt ice, thus reducing the mixed layer salinity and increasing the static stability of the system. Heat lost from the SML by conductive fluxes through the ice or directly to the atmosphere through leads, however, has little influence on S_{SML}. Consider a solid ice cover (0% leads) overlying a weakly-stratified upper ocean with $S_{SML}<S_*$. Because it is weakly stratified, we expect there to be some level of background heat flux from the pycnocline to the SML, by a combination of diffusive convection and SML entrainment processes. Now allow the salinity to slowly rise, e.g., driven by a slow ice growth. Entrainment fluxes rise because of the buoyancy loss at the surface, and diffusive-convective fluxes rise because of the reduction in the typical upper-ocean density ratio (R_ρ). Higher heat fluxes can lead to a new equilibrium by opposing the further growth of ice: this can all be accomplished in models with linear equations of state [*Martinson*, 1990; *Walin*, 1993]. Part of the equilibrium solution involves a "steady-state" conductive flux through the ice, which will be primarily a function of ice thickness and snow cover since the changes in T_{SML} are small compared with the difference between T_{SML} and T_{air}. Now, however, consider a rapid rise in S_{SML}, perhaps caused by advection, as in the present case. The result, as we have seen, can be a catastrophic release of heat into the SML on a time scale that is much shorter than the ice's ability to reach a new steady-state conductive heat flux. The ultimate influence of this process then becomes a competition between the ice that can be melted as the SML temperature anomaly is removed, and the increased stability of the SML by the incorporation of the fresh water from the melted ice.

The present event, which we are postulating is due to cabbeling, occurs in a region where thermohaline steps already exist, although we are not able to determine whether the principal mechanism of initial step formation is diffusive convection or cabbeling. Hence, some diffusive-convective transport of heat and salt occurs through the interface separating the surface layer from the first subsurface layer. Furthermore, intermittent shears are found across this interface, and appear to be associated with baroclinic tides and other internal gravity waves in this region [*Stanton et al.*, 1998]. We have estimated the thermal diffusivity (K_T) through these interfaces based on microscale temperature measurements, which suggest that, in the absence of entrainment from surface stress and ignoring the cabbeling-favorable periods, $K_T \approx 1\text{-}2 \times 10^{-5}\ m^2\ s^{-1}$. The implied rate of heat transport through the interface is therefore about 5-10 W m^{-2} due to shear instabilities and diffusive convection: this value is approximately doubled by the addition of the intermittent entrainment events driven by the wind-driven ice motion during storms. With these background numbers, it is clear that cabbeling events, which transport >100 W m^{-2} upwards during their active lives, could conceivably be important to regional averages of heat flux, even if they are quite rare.

3. Regional Observations Of Cabbeling-Like Steps

From the analyses presented in the previous section, it is clear that a cabbeling-like convective event can transfer a large amount of heat from the WDW to the SML: our estimate for the one event was ~300 W m^{-2}, averaged over a 6 h period. Since the basin-averaged upward heat flux required to balance the WDW heat budget for the Weddell Sea is about 20 W m^{-2} [*Fahrbach et al.*, 1994], only a small fraction of the Gyre needs to be actively cabbeling to provide a significant fraction of the total heat flux. The two large cabbeling events occupy 5-10% of the drift track length. Taking 5% as the cabbeling-active area, the cabbeling contribution to the regional average heat flux is about 20 W m^{-2}, based solely on our **ANZFLUX** data. The area surrounding Maud Rise may be a preferred site for cabbeling however, since the Taylor column circulation over the Rise provides the high-salinity SML that appears to provide the trigger, *via* advection, for the cabbeling instability.

Cabbeling-like layers have been found in many locations throughout the Weddell Gyre [*Foster*, 1972; *Foster and Carmack*, 1976; *Muench et al.*, 1990; *Muench*, 1991; *Foster*, 1994]. In many cases, the interface separating these layers from the SML, or the remnant winter mixed layer when summer surface restratification is present, consists of a sequence of smaller diffusive-convective steps, through which the estimated diapycnal flux is only about 1-2 W m^{-2} [*Muench et al.*, 1990]. The presence of such steps is usually assumed to indicate that other mixing processes are not active [*Melling et al.*, 1984; *Padman*, 1995], so that the effective total diffusivity in the pycnocline between the SML and the cabbeling-like layer is small. We believe that, under these circumstances, the system can be treated as a “traditional” diffusive-convective staircase (see also, *Rudels* [1991]). There is another interesting twist to the process in this environment, however. As *Foster* [1994] noted, the pressure dependence in $\alpha(S,T,P)$ slightly decreases the slope of $(\partial T/\partial S)_2$ as P increases, so that S_*, the minimum cabbeling-favorable SML salinity, is decreased also. That is, if some process depresses the pycnocline sufficiently, an interface that is initially slightly stable to cabbeling ($S_{SML}<S_*$) can become unstable ($S_{SML}\geq S_*$), possibly initiating a new catastrophic convective event. *Foster* [1994] proposed that baroclinic semidiurnal tides could cause this depression: downwelling at the Gyre margins could also act as a trigger for renewed cabbeling activity. However, once the cabbeling layers are no longer in direct communication with the air/sea interface via the SML, it is expected that the T and S structure will adapt to any periodic depression, preventing further cabbeling activity for the same depth change.

3.1. Recent Observations of Cabbeling-like Layers

CTD profiles from several recent cruises that were not included in the review by *Muench* [1991] are now available to improve our definition of the most likely locations for cabbeling to occur. We discuss each of these data sets separately below. In addition, we reconsider data that has already been used by *Muench et al.* [1990] to investigate diffusive convection in the northwestern Weddell Sea. Cruise locations are indicated on **Figure 9.**

ANT-VIII/2: This 1989 cruise of the “Polarstern” [*Augstein et al.*, 1991] found large steps along a transect from about 70°S, 15°W, to 66°S, 35°W. The largest steps, about 100 m thick, were located near 67.2°S, between 22°W and 26°W. This region, which we call the Central Gyre, was found to contain step structures as early as 1973 [*Foster and Carmack*, 1976].

ANT-IX/2: This 1990 cruise of the “Polarstern” [*Bathmann et al.*, 1992] found large steps along a transect from about 68°S, 21°W, to 66.2°S, 30.2°W. The largest steps, about

120 m thick, were located near 66.9°S, 25.5°W, i.e., very close to the largest steps found in *ANT-VIII/2*.

ANT-X: This 1992/93 cruise of the "Polarstern" [*Bathmann et al*., 1994] found large steps along a transect from about 68.8°S, 18°W, to 66.2°S, 31.3°W. The largest steps, about 50 m thick, were located between 68.8°S, 18°W, and 67.8°S, 21°W, i.e., southeast of the largest steps found in *ANT-VIII/2* and *ANT-IX/2*. Large steps were also found at three stations over the continental slope further east, near 69°S, 7°W. While these layers occurred in a small region, they have the same basic characteristics as the Central Gyre steps.

A-23: This 1995 WOCE southern ocean section obtained approximately forty CTD stations in the Weddell Sea, and passed through the area in which the three "Polarstern" cruises discussed above had found steps. However, while a few profiles showed some step structure, none displayed the thick layers that we believe are characteristic of cabbeling. These observations indicate that temporal variability does occur, although we are not able at present to unequivocally determine whether the variations represent seasonal or interannual changes.

Ameriez: The 1986 program in the northwestern Weddell Sea [*Husby and Muench*, 1988] obtained several CTD casts through an extensive area of steps [*Muench et al.*, 1990], in a region from about 66°S to 64.5°S, and from 42°W to 50°W. Steps have also been observed in this region in 1991 and 1992 [*Foster*, 1994].

As has been recognized since the work by *Fofonoff* [1956], and more clearly illustrated by *Foster* [1972] and *Foster and Carmack* [1976], large steps are nearly always associated with a marginally-critical *T*-*S* curve, i.e., $S_{SML} \approx S_*$ (see **Figure 1** and **Figure 7**). This is not always true: several of the *Ameriez* profiles have S_{SML} significantly less than S_*. In these cases the interface between the SML and the cabbeling-like layer is composed of the small Type A steps that are believed to transport only 1-2 W m^{-2} of heat upward [*Muench et al.*, 1990]. In general, these Type A steps are absent in this interface when $S_{SML} \approx S_*$. Based on this observation, we interpret the large steps in the *Ameriez* data as examples of "relict" cabbeling layers: i.e., layers that were formed when the *T*-*S* characteristics were cabbeling-favorable ($S_{SML} \approx S_*$), and that are now better regarded as low-density ratio diffusive-convective steps. As we noted above, however, these layers may be reinvigorated by subsequent resalinization of the SML (e.g., in the following winter), or by downwelling following the suggestion of *Foster* [1994], in which the pressure-dependence in $\alpha(S,T,P)$ reduces the density ratio when the depth of a diffusive-convective interface is increased.

3.2. Relationship of Steps to Basin-Scale Ice Cover Variations

The variation in step characteristics in the central Gyre, near 67°S, 25°W, is associated with the salinity of the SML or remnant winter layer. This correlation suggests that steps might only be formed when sufficient local ice growth occurs to create the high-salinity surface layer. For the central Gyre, the wind stress curl that drives the ice divergence (and oceanic upwelling) may need to be sufficiently strong to advect the locally-formed ice away from the central Gyre and allow increased ice growth. We therefore investigate the interannual variability of ice concentration (C_{ice}) derived from the Special Sensor Microwave Imager (SSM/I: see, e.g., *Gloerson et al*., 1992). In **Figure 10**, daily estimates of C_{ice} from 67°S, 25°W are plotted as a function of day-of-year (DOY) for the period August 1987 to August 1995. Concentration for each year has been offset vertically by 20% ice cover. During the winter period (roughly DOY 170 to 300), C_{ice} is usually 90±5%. The “summer”, ice-free period lasts from about DOY 25 to day 85. The most obvious difference between years occurs in the timing of onset of high C_{ice}, which occurs as early as DOY 85 in 1991, and as late as DOY 135 in 1988 and 1990. In general, ice forms earlier than average for 1991-1992, and 1994-1995, and later than average for 1988-1990 and 1993. We note that the two cruises for which large steps were found were in 1989 and 1990, when ice onset occurred late (mid-April), and the A-23 cruise in 1995 obtained data after a relatively long winter-ice year.

What is the physical link between timing of ice onset and the presence of steps? Strong surface cooling begins in this region in March. Once an ice cover is established, the rate of heat loss drops abruptly, as does the flux of salt. If this occurs early in the fall, the final SML salinity will be lower than if cooling continues until late fall. Of course, we have assumed here that the interannual variability in ice cover is determined more by atmospheric effects than by oceanic feedback: some of the interannual variability in ice concentration may well be caused by preconditioning of the ocean, either by the previous winter's convective activity or by the amount of seasonal stratification attained during the most recent summer. Nevertheless, the relationship between the underlying hydrographic state and interannual sea ice variations suggests that the presence of steps depends to some extent on the interaction of the ice cover and the upper ocean.

The variation of sea ice concentration in the Weddell Sea appears to be part of a circum-Antarctic oscillation, with a period of about 8 years (see *Murphy et al.* [1995] and included references). The causes of this oscillation are beyond the scope of the present study, however we note that the apparent connection between ice conditions and the likelihood of cabbeling in the Central Gyre supports our view that ocean fluxes will vary with a similar time scale. That is, upper-ocean variability is expected on the same time scale as the sea-ice variations, without regard to the interactions that might drive this relationship.

3.3. Advection

Muench [1991] suggested that the steps observed in the northwestern Weddell Sea might occur in parcels of water where convective activity had occurred elsewhere in the Gyre, followed by advection into the observation region. Water in the Weddell Sea circulates, to first order, in a basinwide, cyclonic gyre. Mean current speeds overlying the continental slopes surrounding the central, deep basin have been measured at some locations over periods up to several years, and are typically 5-10 cm/s in the 200-250 m depth range [*Bersch et al.*, 1992; *Fahrbach et al.*, 1994; *Muench & Gordon, 1995*]. The observed large staircase features have been situated, however, in the basin seaward of the slope currents. If we assume that the staircase features form initially by way of upper layer processes associated with Maud Rise, as postulated above, then a mechanism is required by which the features can be advected westward into the central Weddell Gyre where they have been observed.

Observations of mean currents in the central basin are few. We present, instead a plot showing particle pathways computed at 222 m depth using results from a recently updated version of the Semtner-Chervin POCM [*Semtner & Chervin*, 1992] (Figure 11). The version used was an ocean-only model (as compared to a coupled ice-ocean model) driven by ECMWF wind fields.

The modelled circulation is consistent with what little we know, based on measurements, of the currents near Maud Rise and westward. *Bersch et al.* [1992] measured south-southwestward mean currents over several months near 200 m depth just west of Maud Rise. A short (7-day) time series of measurements obtained during the summer 1994 AnzFlux experiment revealed mean south-southwestward flow [*Muench*, 1996]. The currents are nonuniform across the basin, with roughly zonal meandering westward jets through the central basin centered near 67 and 70°S. Mean westward speed in these jets is about 5 cm/s, as compared to vanishingly small speeds outside the jets. Reference to the regional bottom topography [GEBCO chart dated 1981] shows that the jets parallel regions of slightly increased bottom slope. Their presence is consistent with a strongly barotropic circulation wherein the mean circulation tends to parallel isobaths.

If we assume for the sake of argument that the modelled streamlines are valid, then the following can reasonably be suggested. The staircase features are distributed consistent with formation near Maud Rise followed by westward advection in the jets. At a speed of order 5 cm/sec, consistent with the model and available field results, it would take roughly 20 months for features to migrate west from a formation area on the eastern flank of Maud Rise to the westernmost observed site ("A,B") near 65°S and 40-45°W. Since 5 cm/sec is a maximum westward speed, actual migration times would probably be longer. The staircases appear to come to rest in the western basin preferentially in regions of near-zero currents. Presumably they remain at these locations and evolve continuously through double diffusive processes until they are disrupted by turbulence, possibly generated by an energetic transient current event.

4. CONCLUSIONS

The principal characteristics of the Maud Rise cabbeling event that we described in section 2 are as follows.

1. The event was initiated by advection of a relatively salty surface mixed layer (SML) over a core of WDW flowing around Maud Rise. The consequent reduction in static stability was sufficient to create marginally cabbeling-favorable conditions.
2. During the ~6 h event, the mean upward heat flux is estimated at 65-350 W m^{-2}, based on measurements of the dissipation rate of turbulent kinetic energy, the change in temperature of the SML, and the properties of the convecting layer.
3. The convective time scale in the mixing event was about 10^3 s, which was also seen in the displacement of the underlying pycnocline. The maximum vertical extent of the mixing patch was about 100 m. We estimate a vertical velocity scale for the layer convection of about 1 cm s^{-1}.
4. Most mixing in a cabbeling event occurred in the weak stratification below the sharp pycnocline. However, the pycnocline did become unstable, allowing effective mixing between the SML and the lower pycnocline. The entrainment of SML fluid into the pycnocline caused an elevation of the sharp pycnocline, which therefore increases its exposure to SML entrainment driven by surface stress and convection.

The time and velocity scales of the event are intriguingly close to estimates by *Foster* [1972], that were based on numerical solutions of a two-dimensional linear instability analysis. The high local heat fluxes implicate this process as a possibly significant component of the mean heat loss from WDW to the surface layer, and ultimately to the ice and atmosphere.

The regional distribution of cabbeling-like features was then reviewed. Based solely on the **ANZFLUX** measurements from the second drift camp near Maud Rise, we estimate that these features occupy about 5-10% of the region. CTD surveys elsewhere in the Weddell Sea indicate that cabbeling-like layers are usually found along the line of most strongly upwelled WDW, i.e., the axis of the Weddell Gyre. In several observations, the necessary hydrographic conditions for cabbeling are not satisfied. We suggest that these layers are relict features that were originally created by energetic cabbeling, but are now maintained as steps by less-active “regular” diffusive convection.

We propose two possible explanations for the observed locations of large layers. Cabbeling might either require close contact between the WDW and a saline surface layer; or, cabbeling might only be found in water that has been modified in the Maud Rise region, then subsequently slowly advected westward in the central Gyre. Repeated CTD surveys (approximately annually for several years) through the central Gyre suggest that cabbeling-like layers are intermittent in time, and we have hypothesized that a link exists between their variability and the interannual variations in sea ice extent.

Based on these observations, the relatively good success of models used to predict upper-ocean heat fluxes seems somewhat serendipitous. Inclusion of the cabbeling mechanism in models would lead to better representation of instantaneous fluxes, and provide improved understanding of the relationships between ice formation, upwelling, and high heat flux events. Our analysis of a single cabbeling event suggests that, at least as the cabbeling-critical point of $S_{\mathrm{SML}}=S_*$ is approached, adequate representation of upper ocean fluxes requires the use of a non-linear equation of state that can incorporate the cabbeling instability.

In some ways the diapycnal cabbeling instability simply represents a limit of double-diffusive convection, as postulated by other authors [*McDougall*, 1981a,b; *Rudels*, 1991]. There are, however, two ways in which this view is invalid. First, unlike double diffusion, diapycnal cabbeling can occur without requiring that the effective diffusivities of heat and salt are different. Secondly, our observations suggest that cabbeling is an intermittent, catastrophic process with heat fluxes within an active event exceeding 100 W m^{-2}, whereas diffusive-convection is usually thought of as a fairly continuous process generating modest fluxes (in the Maud Rise region, $O(10)$ W m^{-2}). The influence of intermittency in the upward heat flux on the thermodynamics of the SML and sea ice cover should be investigated: while continuous fluxes of, say, 10 W m^{-2} can be transported conductively through the ice and snow cover to the atmosphere, an intermittent flux of 300 W m^{-2} must result in ablation of the ice base, and thus at least a temporary freshening of the mixed layer salinity. This process may, indeed, be what finally terminates the cabbeling event: if the upward salt flux from the pycnocline into the SML is less than the freshwater flux from newly-melted ice, then S_{SML} is decreased such that it is again less than S_*, and cabbeling can no longer occur.

Acknowledgments: We thank Karen Heywood for providing the WOCE A-23 CTD data, and Bert Semtner, Julie McClean, and Robin Tokmakian for model annual-averaged velocity fields for Lagrangian particle tracking. We are grateful to Bruce Huber and Doug Martinson for providing the LDEO yo-yo CTD data. This work was supported by the National Science Foundation, Office of Polar Programs, through grants OPP-9317321 to OSU (LP), and OPP-9315019 to ESR (RDM).

References

Augstein, E., N. Bagriantsev, and H. W. Schenke (Eds.), *The Expedition ANTARKTIS VIII/1-2, 1989, with the Winter Weddell Gyre Study of the Research Vessels "Polarstern" and "Akademik Federov", Ber. Polarforsch., 84*, Alfred-Wegener-Institut, Bremerhaven, 1991.

Baker, M. A., and C. H. Gibson, Sampling turbulence in a stratified ocean: statistical consequences of strong intermittency, *J. Phys. Oceanogr., 17*, 1817-1836, 1987.

Bagriantsev, N. V., A. L. Gordon, and B. A. Huber, Weddell Gyre: temperature maximum stratum, *J. Geophys. Res., 94*, 8331-8334, 1989.

Bathmann, U., M. Schulz-Baldes, E. Fahrbach, V. Smetacek, and H.-W. Hubberten (Eds.), The Expedition ANTARKTIS IX/1-4, of the Research Vessel "Polarstern" in 1990/91, *Ber. Polarforsch., 100,* Alfred-Wegener-Institut, Bremerhaven, 1992.

Bathmann, U., V. Smetacek, H. de Baar, E. Fahrbach, G. Krause (Eds.), The Expedition ANTARKTIS X/6-8, of the Research Vessel "Polarstern" in 1992/93, *Ber. Polarforsch., 135*, Alfred-Wegener-Institut, Bremerhaven, 1994.

Bersch, M., G. A. Becker, H. Frey, and K. P. Koltermann, Topographic effects of the Maud Rise on the stratification and circulations of the Weddell Gyre, *Deep Sea Res., 39*, 303-331, 1992.

Bowman, M., and A. Akubo, Cabbeling at thermohaline fronts, *J. Geophys. Res., 83*, 6173-6178, 1978.

Deardorff, J. W., and G. E. Willis, Turbulence within a baroclinic laboratory mixed layer above a sloping surface, *J. Atmos. Sci., 44*, 772-778, 1987.

Dillon, T. M., Vertical overturns: a comparison of Thorpe and Ozmidov length scales, *J. Geophys. Res., 87*, 9601-9613, 1982.

Fahrbach, E., G. Rohardt, M. Schröder, and V. Strass, Transport and structure of the Weddell Gyre, *Ann. Geophysicae, 12*, 840-855, 1994.

Fahrbach, E., M. Schröder, and A. Klepikov, Circulation and water masses in the Weddell Sea, *A contribution to the summer school in Savonlinna, 1994*, (needs updating), 1998.

Federov, K. N., On the role of densification during mixing in the dynamics of ocean fronts, *Doklady AN SSSR, 261*, 985-988, 1981.

Flanagan, R., and T. Yulsman, On thin ice, *Earth, 5*, 44-51, 1996.

Fofonoff, N. P., Some properties of sea water influencing the formation of Antarctic bottom water, *Deep Sea Res., 4*, 32-35, 1956.

Foster, T. D., An analysis of the cabbeling instability in seawater, *J. Phys. Oceanogr., 2*, 294-301, 1972.

Foster, T. D., Large, steplike temperature and salinity structures observed in the central Weddell Sea, *Antarctic J. United States*, *XXIX(5)*, 99-100, 1994.

Foster, T. D., and E. C. Carmack, Temperature and salinity structure in the Weddell Sea, *J. Phys. Oceanogr., 6*, 36-44, 1976.

Garrett, C., and E. Horne, Frontal circulation due to cabbeling and double diffusion, *J. Geophys. Res., 83*, 4651-4656, 1978.

Gloerson, P., W. Campbell, D. Cavalieri, J. Comiso, C. Parkinson, and H. J. Zwally, Arctic and Antarctic Sea Ice, 1978-1987: Satellite passive microwave observations and analysis, *NASA Spec. Publ. 511*, 1992.

Gordon, A. L., and B. A. Huber, Southern Ocean winter mixed layer, *J. Geophys. Res., 95*, 11,655-11,672, 1990.

Gregg, M. C., Diapycnal mixing in the thermocline: A review, *J. Geophys. Res*., *92*, 5249-5286, 1987.

Husby, D. M., and R. D. Muench, Hydrographic observations in the northwestern Weddell Sea marginal ice zone during March 1986, NOAA Tech. Memo. NOAA-TM-NMFS-SWFC-106, 33 pp. [available from SW Fish. Ctr., NOAA/NMFS, Monterey, CA 93942.], 1988.

Kil'matov, T. R., and V. A. Kuz'min, Effect of cabbeling in the mixing of sea water and it's seasonal manifestation on the Pacific Ocean subarctic front, *Izvestiya, Atmos. and Oceanic Physics, 27*, 628-631, 1991.

Linden, P. F., and T. G. L. Shirtcliffe, The diffusive interface in double-diffusive convection, *J. Fluid Mech., 87,* 417-432, 1978.

Martinson, D. G., Evolution of the Southern Ocean winter mixed layer and sea ice: Open ocean deepwater formation and ventilation, *J. Geophys. Res., 95*, 11,641-11,654, 1990.

McDougall, T. J., Double-diffusive convection with a non-linear equation of state. Part I: The accurate conservation of properties in a two-layer system, *Prog. Oceanogr., 10*, 71-89, 1981a.

McDougall, T. J., Double-diffusive convection with a non-linear equation of state. Part II: Laboratory experiments and their interpretation, *Prog. Oceanogr., 10*, 91-121, 1981b.

McPhee, M. G., S. F. Ackley, P. Guest, B. A. Huber, D. G. Martinson, J. H. Morison, R.D. Muench, L. Padman, and T. P. Stanton, The Antarctic Zone Flux Experiment, *Bull. Am. Meteorol. Soc.*, *77*, 1221-1232, 1996.

Melling, H., R. A. Lake, D. R. Topham and D. B. Fissel, Oceanic thermal structure in the western Canadian Arctic, *Continental Shelf Res.*, *3*, 233-258, 1984.

Moum, J. N., Efficiency of mixing in the main thermocline, *J. Geophys. Res*., *101*, 12,057-12,069, 1996.

Muench, R. D., Relict convective features in the Weddell Sea, In: *Deep Convection and Deep Water Formation in the Oceans*, edited by P. C. Chu and J. C. Gascard, Elsevier Science Publishers B.V., 1991.

Muench, R. D., Upper layer current measurements in the eastern Weddell Sea during winter, *Antarctic J. United States*, *1995 Review*, 1996 (in press).

Muench, R. D., H. J. S. Fernando, and G. R. Stegen, Temperature and salinity staircases in the northwestern Weddell Sea, *J. Phys. Oceanogr., 20*, 295-306, 1990.

Muench, R. D., and A. L. Gordon, Circulation and transport of water along the western Weddell Sea Margin, *J. Geophys. Res., 100*, 18,503-18,515, 1995.

Muench, R.D., and J.H. Morison, Mesoscale features and winter heat fluxes in the eastern Weddell Sea, *J. Geophys. Res.*, submitted April 1998 (subject to author change).

Murphy, E. J., A. Clarke, C. Symon, and J. Priddle, Temporal variation in Antarctic sea ice: analysis of a long term fast-ice record from the South Orkney Islands, *Deep Sea Res.*, *42*, 1045-1062, 1995.

Orsi, A. H., W. D. Nowlin Jr., and T. Whitworth III, On the circulation and stratification of the Weddell Gyre, *Deep Sea Res.*, *40*, 169-203, 1993.

Ou, H. W., Some effects of a seamount on oceanic flows, *J. Phys. Oceanogr.*, *21*, 1835-1845, 1991.

Padman, L., Small-scale physical processes in the Arctic Ocean, In: "*Arctic Oceanography: Marginal Ice Zones and Continental Shelves*", Edited by W.O. Smith and J.M. Grebmeier, Coastal and Estuarine Studies (49), AGU, Washington, D.C., 1995.

Padman, L., and T. M. Dillon, Thermal microstructure and internal waves in an oceanic diffusive staircase, *Deep Sea Res., 36*, 531-542, 1989.

Padman. L., R. A. Robertson, and M. D. Levine, Pycnocline structure and fluxes in the eastern Weddell Sea in winter, *Antarctic J. United States*, 1995 review, (in press).

Robertson, R. A., L. Padman, and M. D. Levine, Fine structure, microstructure, and vertical mixing processes in the upper ocean in the western Weddell Sea, *J. Geophys. Res., 100*, 18,517-18,535, 1995.

Rudels, B., The diffusive interface at low stability: The importance of non-linearity and turbulent entrainment, *Tellus Series A, 43,* 153-167, 1991.

Schmitt, R. W., Double diffusion in oceanography, *Ann. Rev. Fluid Mech., 26*, 255-285,1994.

Stanton, T. P., L. Padman, and R. A. Robertson, Heat fluxes through the permanent pycnocline in the eastern Weddell Sea, submitted to *J. Geophys. Res*., 1998.

Taylor, J., The fluxes across a diffusive interface at low values of the density ratio, *Deep-Sea Res., 35,* 555-567, 1988.

Thorpe, S.A., Turbulence and mixing in a Scottish loch, *Philos. Trans. R. Soc. London Ser. A, 286*, 125-181, 1977.

Turner, J. S., *Buoyancy Effects in Fluids*, Cambridge University Press, New York, 1973.

Walin, G., On the formation of ice on deep weakly stratified water, *Tellus, 45*, 143-157, 1993.

LIST OF FIGURES

Figure 7: Potential temperature ($\theta(z)$) as a function of salinity ($S(z)$) for two profiles: at t=218.33, ('+'), before the cabbeling-like event; and at t=218.58 ('o'), during the event (see Figure 6). The straight dashed line is the tangent to the subsurface layer ("Layer 2") isopycnal (σ_2) at (S_2, θ_2). The isopycnal σ_2 is also shown dashed. Potential densities are evaluated for a reference pressure of 120 dbar.

Figure 8: (a) Faint line: high-resolution vertical profile of potential temperature ($\theta(z)$) from the OSU microstructure profiler (t=218.64). Bold line: Thorpe-reordered profile, on the assumption that potential density increases monotonically with increasing θ over the displayed depth range. (b) Salinity ($S(z)$) and potential density ($\sigma_0(z)$) for the same profile as in (a), with ~1-m resolution. (c) Turbulent kinetic energy dissipation rate, $\log_{10}(\varepsilon(z))$, for the same profile as in (a). The approximate noise floor for this measurement is $3\text{x}10^{-9}$ m^2 s^{-3}.

Figure 9: Location of observations of cabbeling-like layers, after *Muench* [1991]. Also shown are the approximate locations of layers discussed in this paper. The location of the **A-23** WOCE transect, which did not find any cabbeling-like layers, is also indicated.
(A) *Muench et al.* [1990]; (B) *Foster* [1994]; (C) *Huber et al.* [1994]; (D) *Foster and Carmack* [1976]; (E) *Gordon* [1978]; (F) **ANZFLUX** (this paper); (G) **ANT-X** (this paper); (H) *Huber et al.* [1981]; (J) *Bersch* [1988]; (K) **ANT-VIII/2** (this paper);
(L) **ANT-IX/2** (this paper); and (M) **ANT-X** (this paper). Isobaths are indicated in meters.

Figure 10: Annual time series of ice concentration (%), for the period July 1987 to August 1995, derived from SSMI satellite brightness temperature, for the pixel containing 67^{o}S, 25^{o}W, near the locations of cabbeling-like layers found in **ANT-VIII/2** and **ANT-IX/2**. Successive years are offset by 20% in the vertical.

Figure 11: Sample particle pathways traced through the annual mean velocity field at 222 m depth in the Semtner/Chervin 1/4^{o} global numerical model. Comparison with the locations of previous observations of cabbeling-like layers suggests that most of these layers are found along pathways traceable eastward to the Maud Rise region.

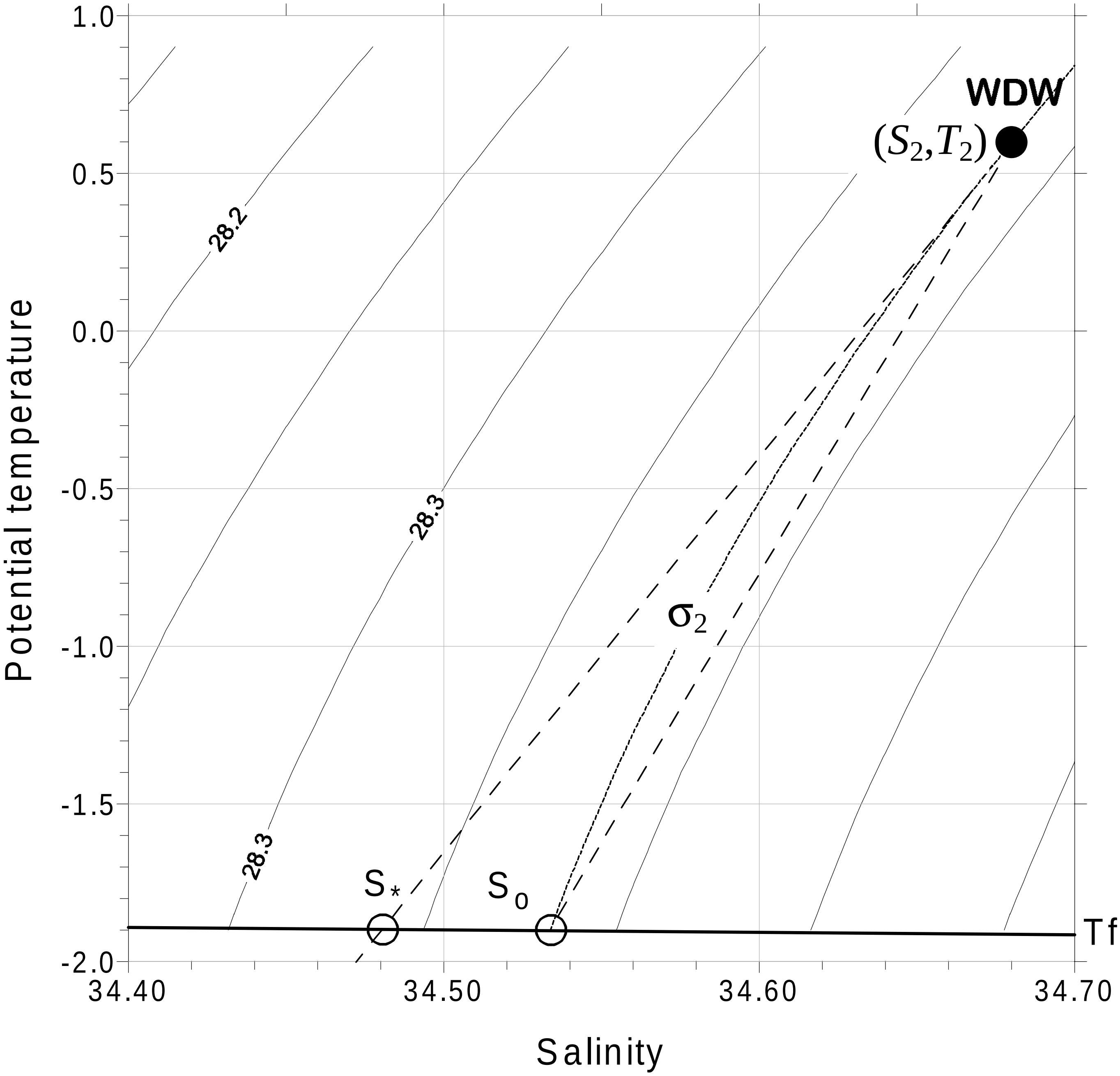

pden_f1.srf
12/19/97 11:38:38

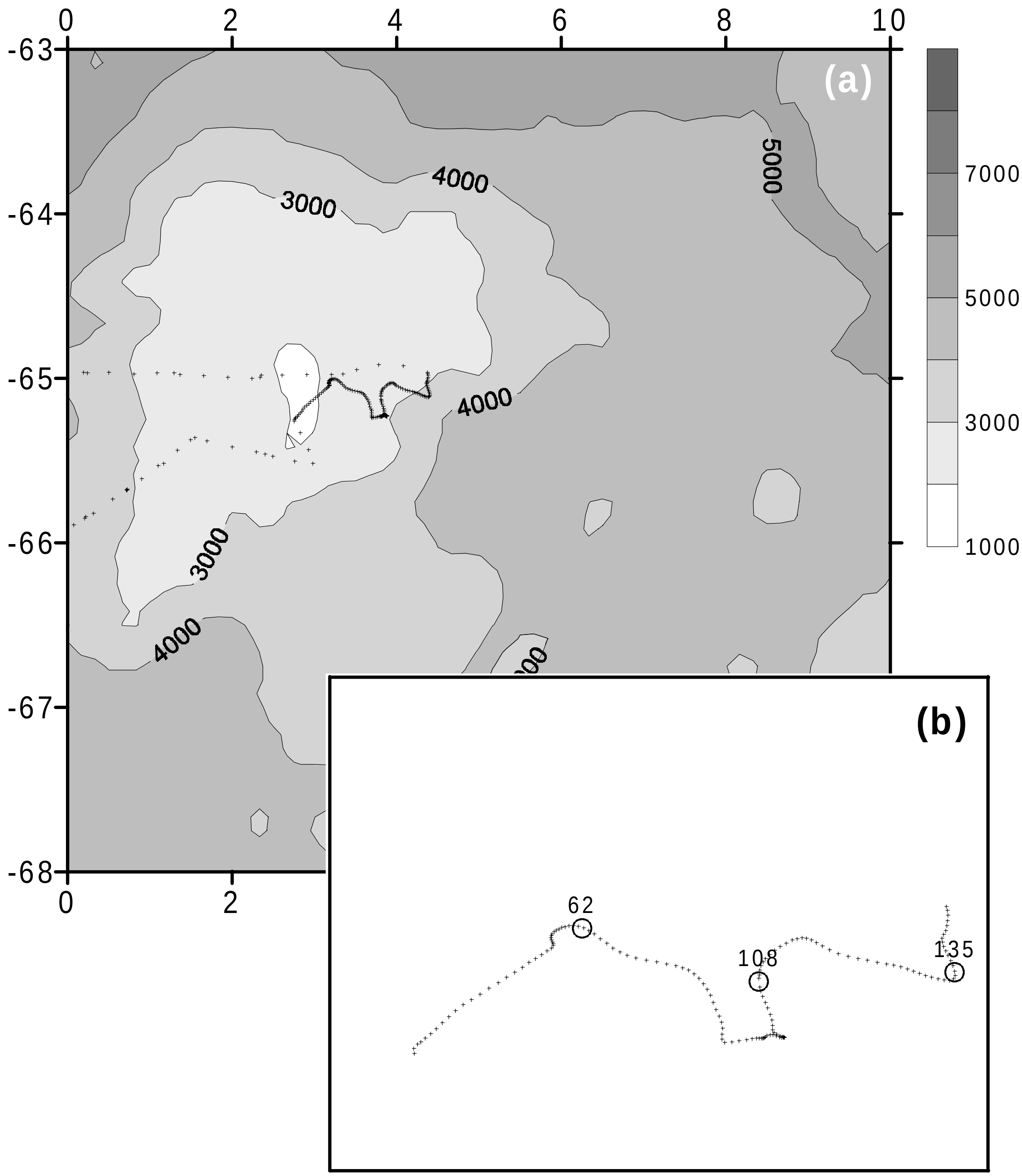

e:/papers/cabbel/maud_top.srf
12/19/97 11:43:11

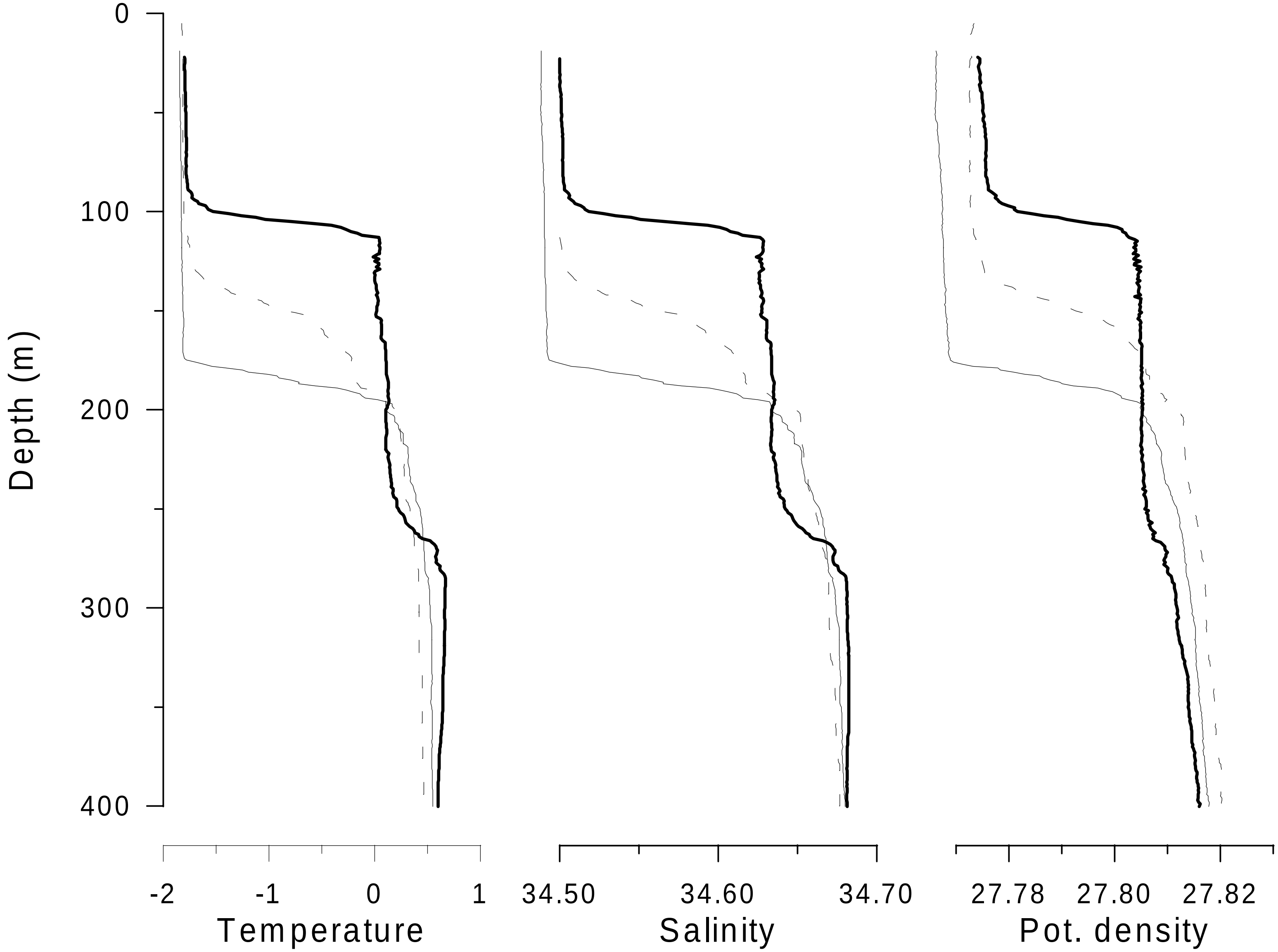
0
100
200
300
400
Depth (m)
-2
-1
0
1
Temperature
34.50
34.60
34.70
Salinity
27.78
27.80
27.82
Pot. density

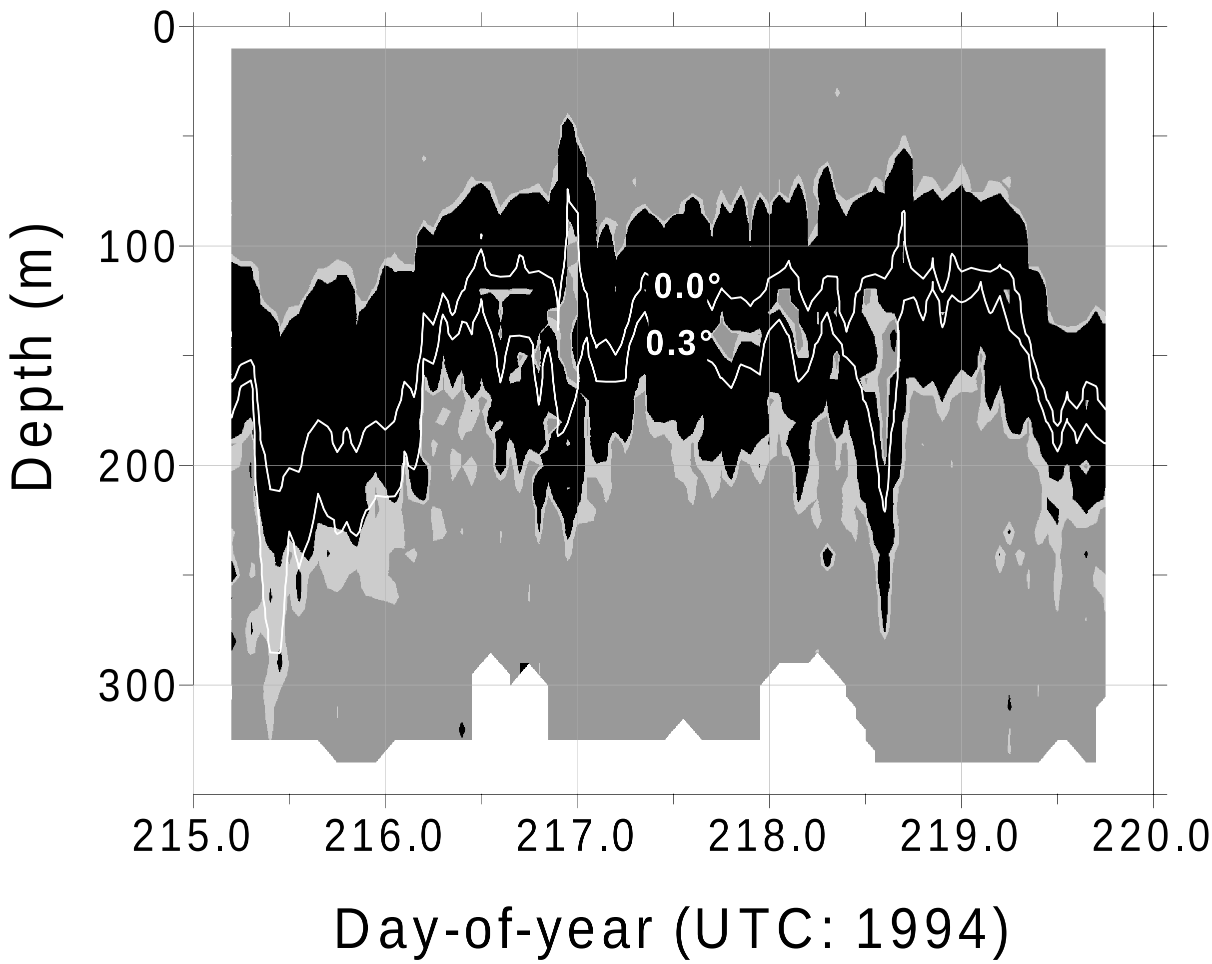

maud_tz2.srf
(in /RSVP/EAV)

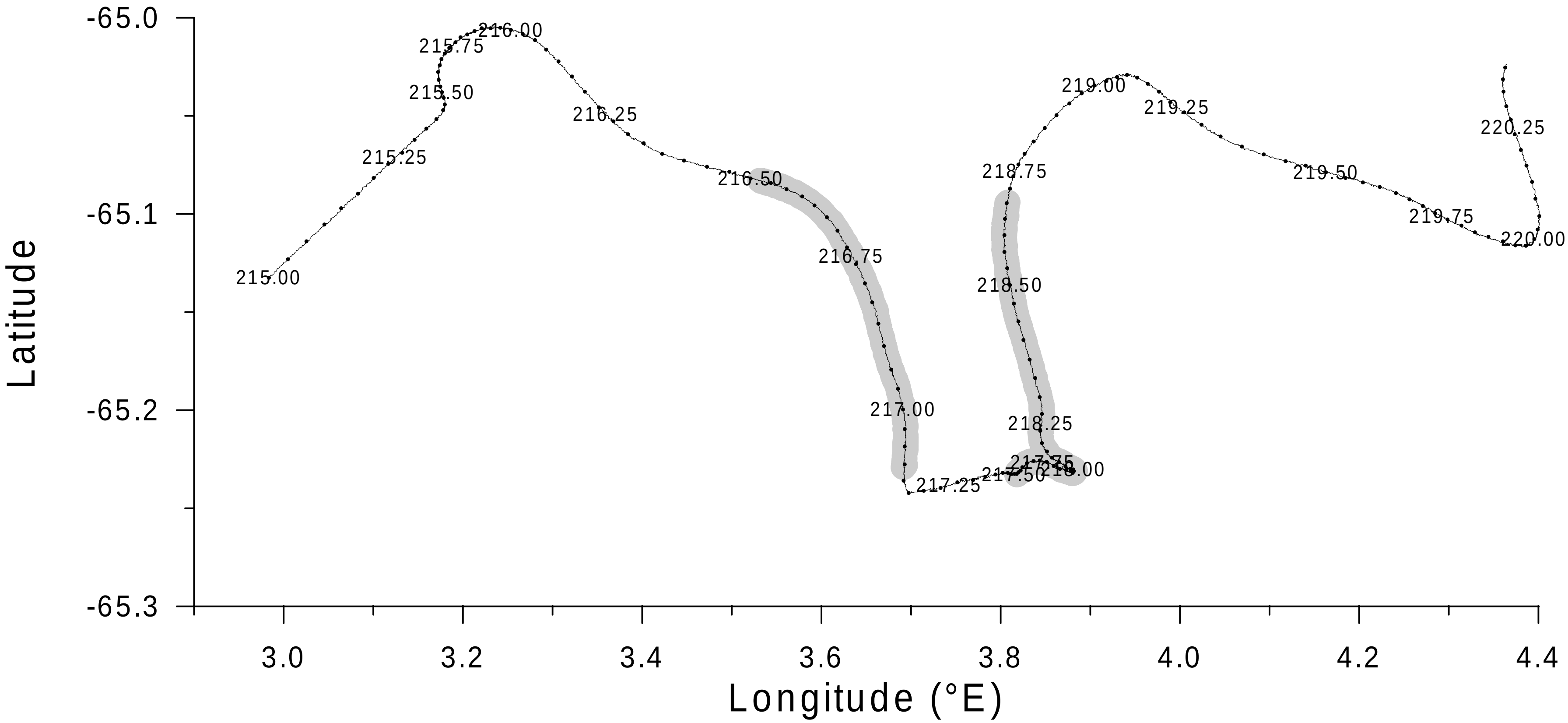

figure5.grf
12/19/97 14:25:02

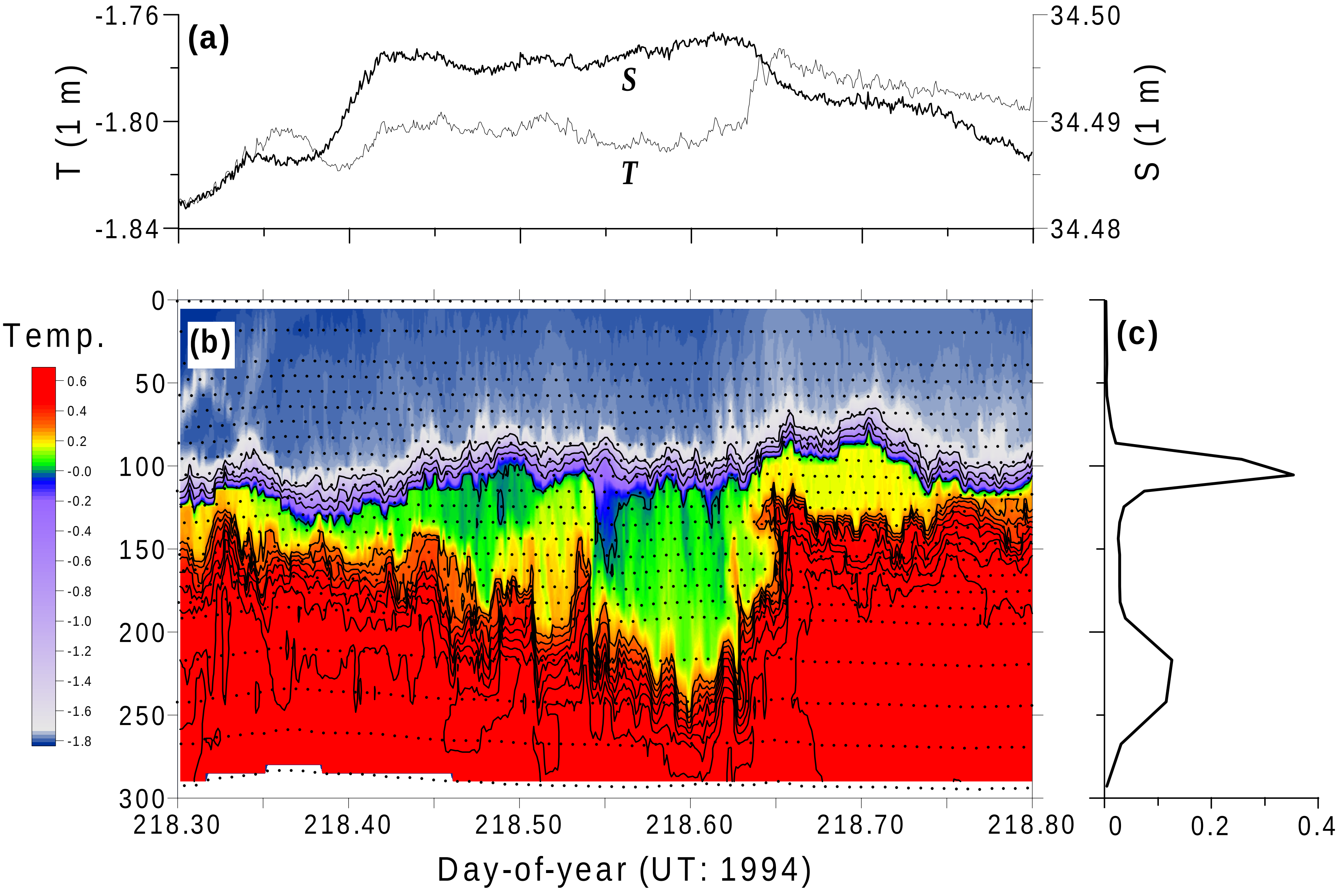

figure6.grf
12/19/97 11:53:26

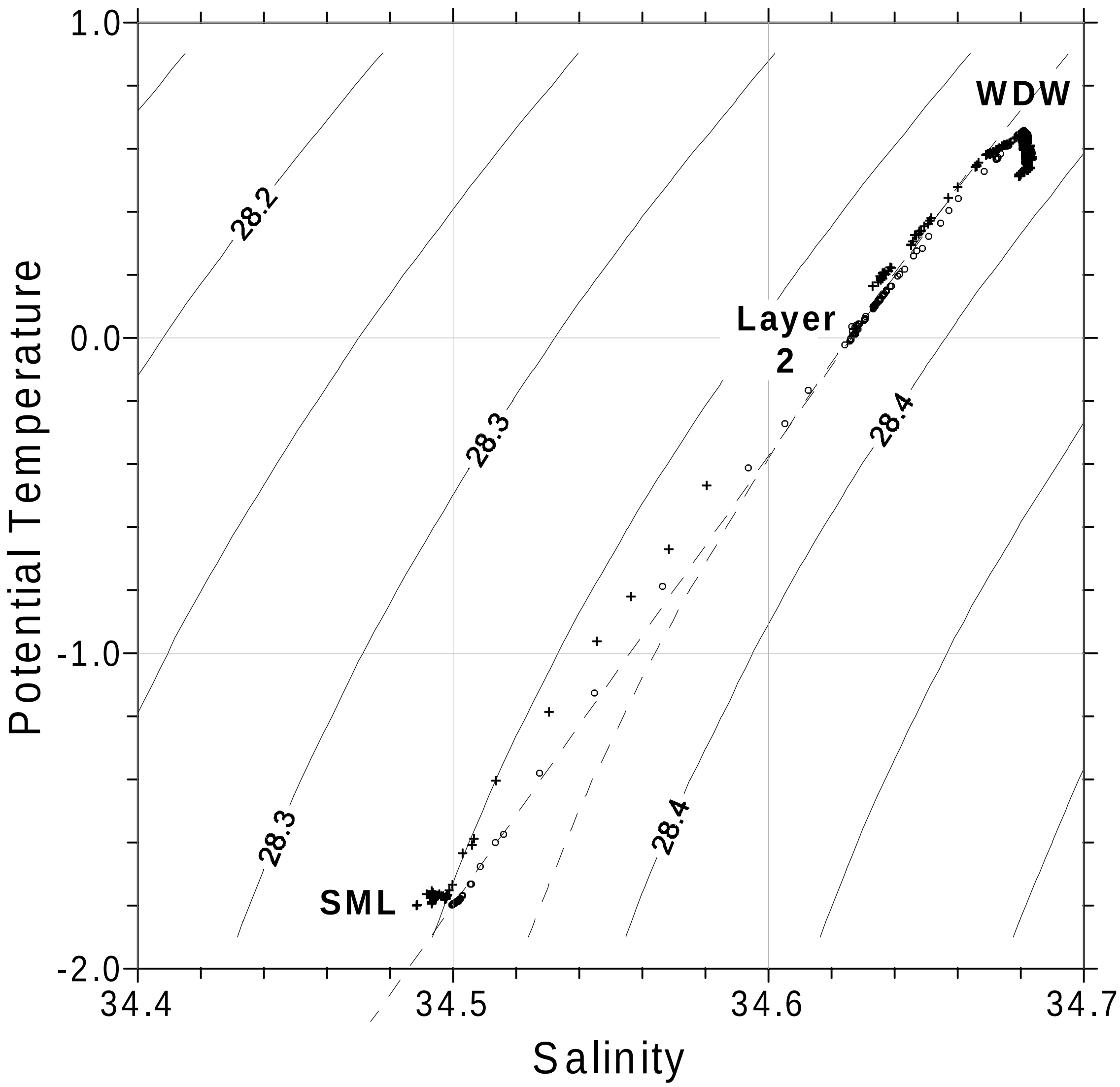

pden_f7.srf
12/19/97 12:00:58

thorpe.grf
12/19/97 12:07:25

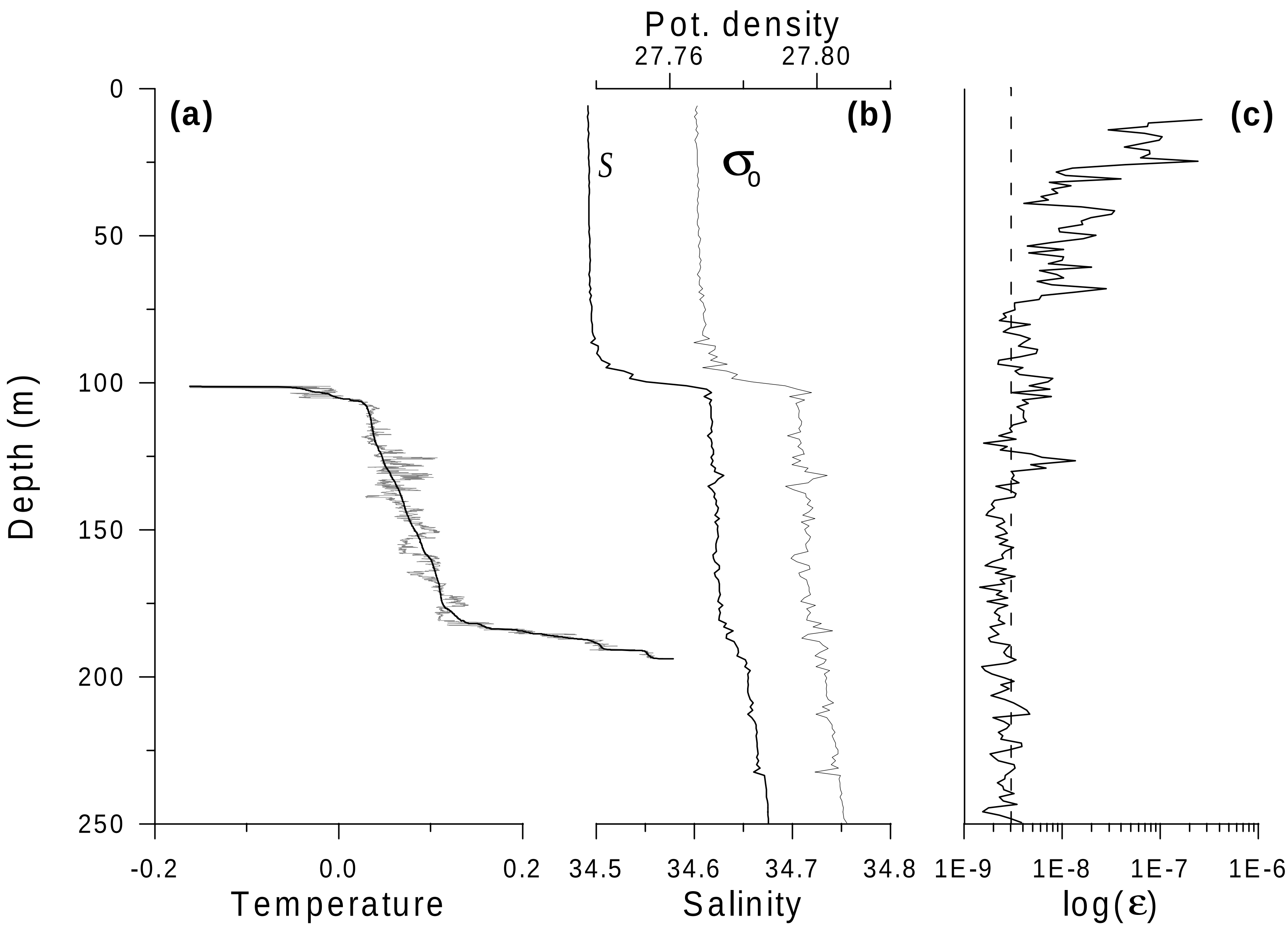

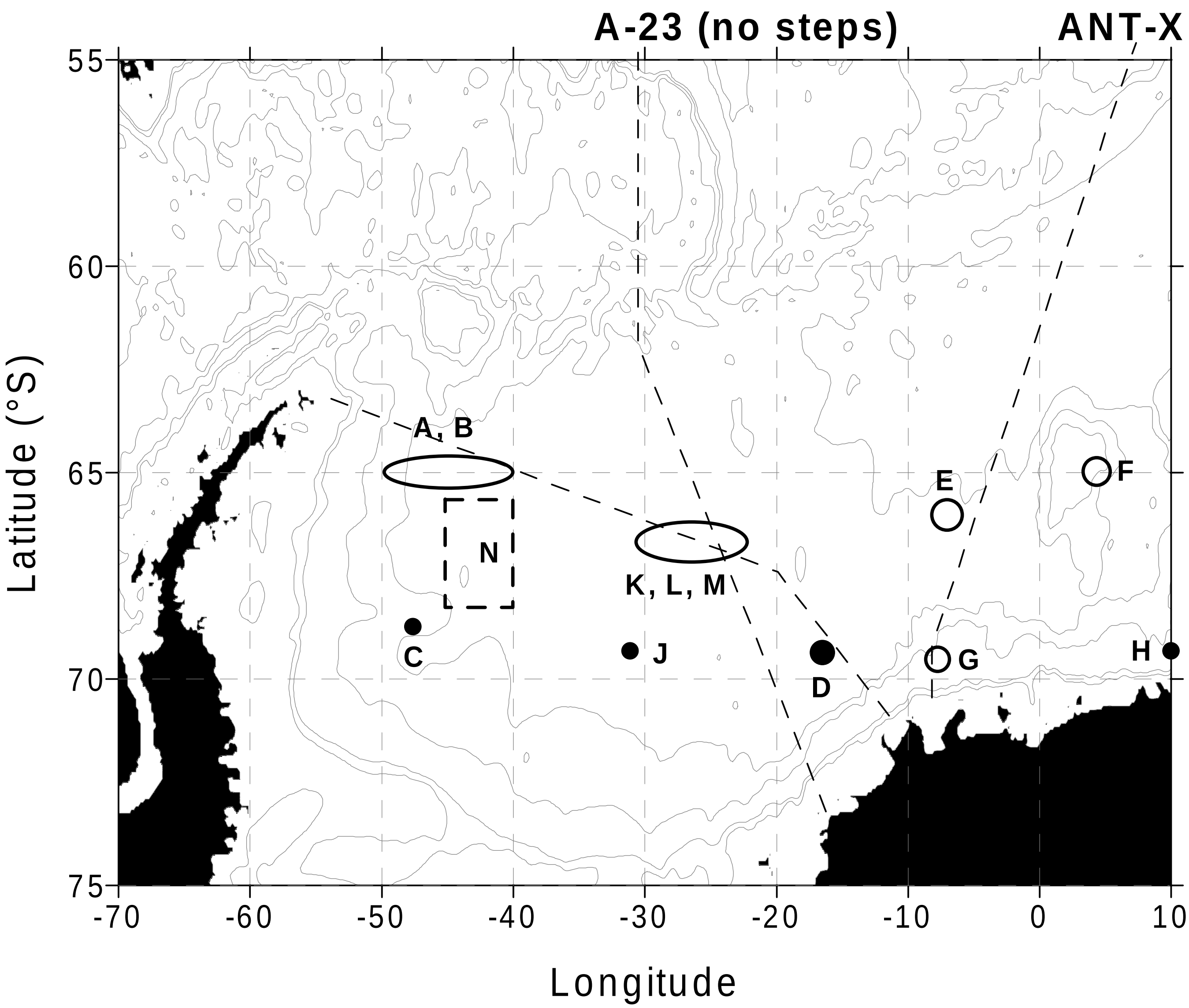

topo_f10.srf
12/19/97 13:46:19

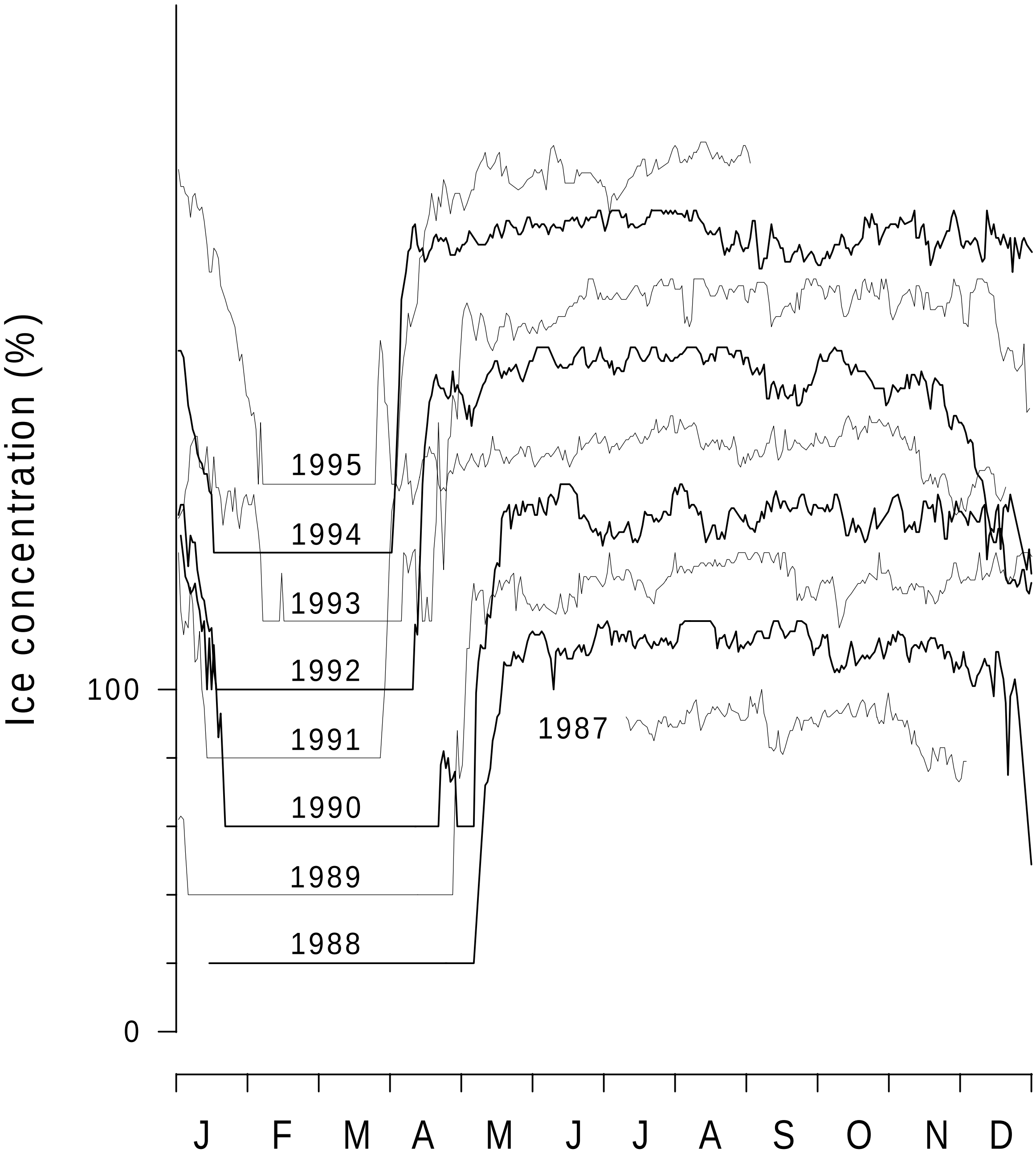

f6725an.grf
12/19/97 13:07:54

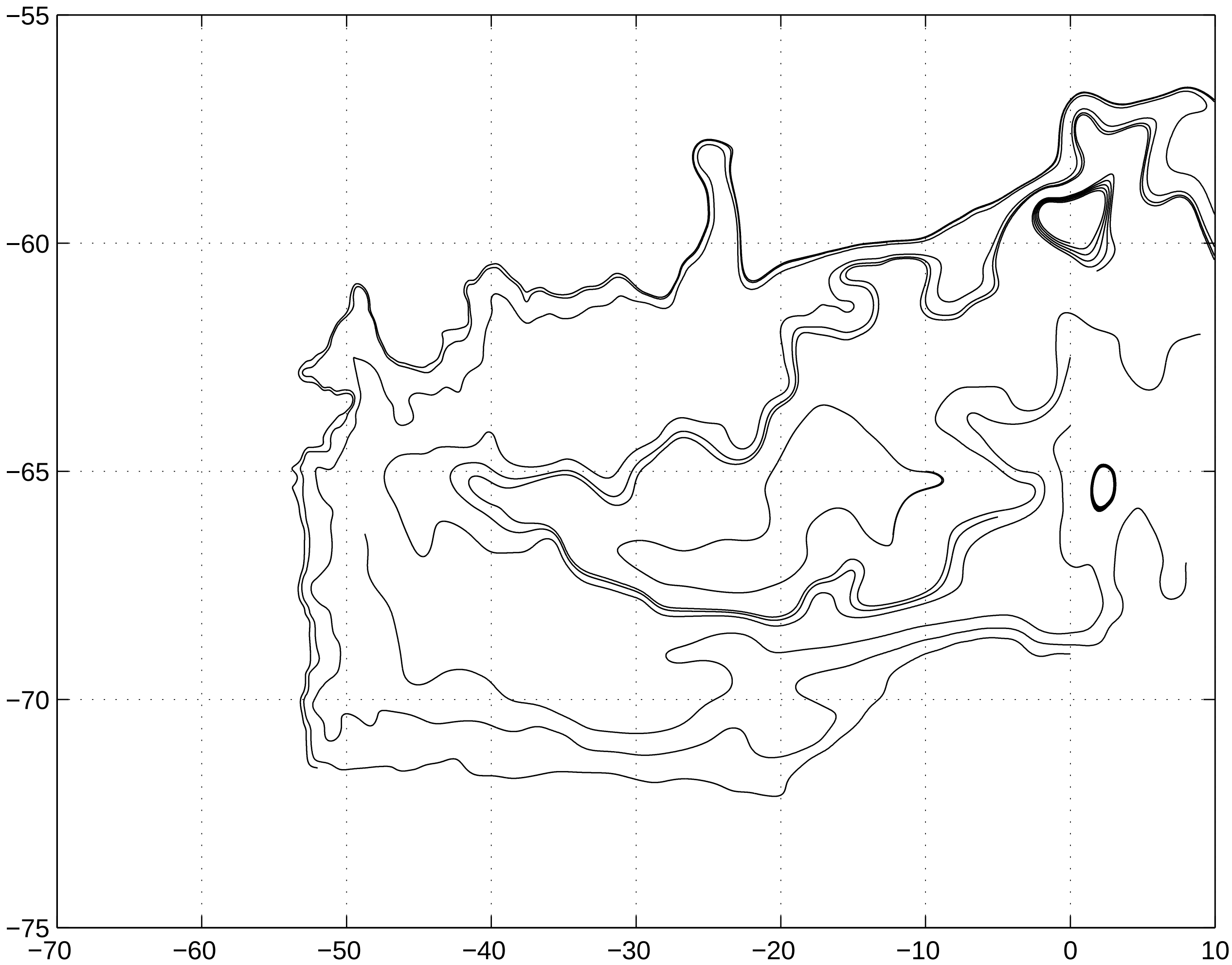
−55
−60
−65
−70
−75
−70
−60
−50
−40
−30
−20
−10
0
10